

Astrophysical Sources of High Energy Neutrinos in the IceCube Era¹

P. Mészáros¹

¹Department of Astronomy & Astrophysics, Department of Physics, Center for Particle and Gravitational Astrophysics, Pennsylvania State University, University Park, PA 16802, U.S.A.; email: nnp@psu.edu

Abstract

High energy neutrino astrophysics has come of age with the discovery by IceCube of neutrinos in the TeV to PeV energy range attributable to extragalactic sources at cosmological distances. At such energies, astrophysical neutrinos must have their origin in cosmic ray interactions, providing information about the sources of high energy cosmic rays, as well as leading to the co-production of high energy gamma-rays. The intimate link with these latter two independently observed types of radiation provides important tools in the search for identifying and understanding the nature of their astrophysical sources. These neutrinos can provide important constraints about the cosmic ray acceleration process, and since they travel essentially unimpeded they can probe our Universe out to the farthest cosmological distances.

1 Very High Energy Neutrino Observations

The exciting discovery [1, 2, 3] of a diffuse flux of TeV to \gtrsim PeV neutrinos of undoubted astrophysical origin was achieved with the cubic kilometer IceCube Cherenkov neutrino detector [4]. This was the culmination of a series of increasingly sophisticated experimental developments and observing campaigns, some previous notable milestones in this search having been undertaken through the Dumand concept [5], the Baikal experiment [6] and the Antares experiment [7].

The flux of very high energy (VHE) neutrinos observed by IceCube includes both cascade events ascribed to $\nu_e, \bar{\nu}_e$, with angular resolutions $\sim 15-30^\circ$, and tracks ascribed to $\nu_\mu, \bar{\nu}_\mu$, with angular resolutions $\sim 1^\circ$. The spectrum clearly departs from that of the atmospheric neutrino background with $\geq 7\sigma$ significance (Fig. 1, left).

The flavor ratio is compatible with a 1:1:1 distribution as expected from pion decay followed by vacuum oscillations across cosmological distances [9] (Fig. 1, right). As far as the directions from which the individual neutrinos arrive to Earth, there is no hint of a concentration towards either the galactic center or the plane, being compatible with an isotropic flux [10]. Neither is there any significant correlation with the arrival direction

¹Preprint - Accepted by Annual Review of Nuclear and Particle Science; to appear in vol. 67 (2017)

Energy Spectrum

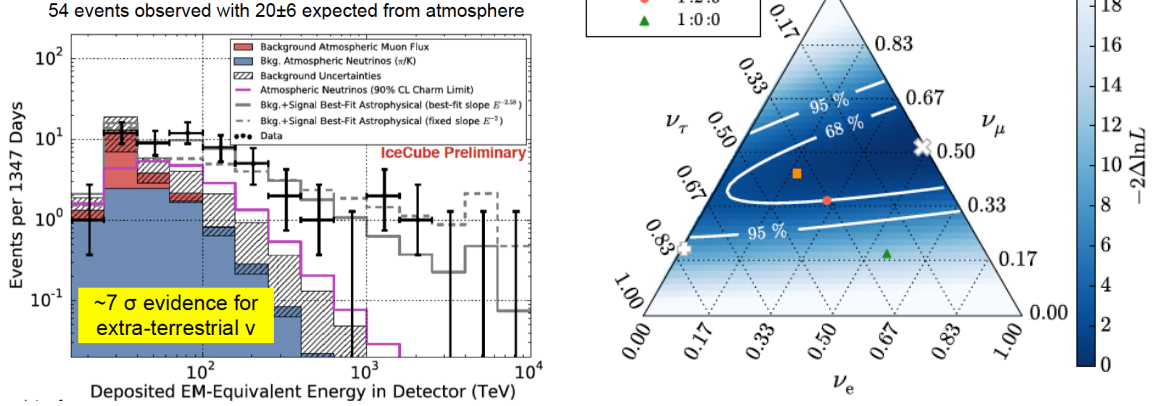


Figure 1: Left: All-flavor spectrum of VHE neutrinos detected by IceCube (from M. Kowalski, in Procs. Neutrino2016, in press; see also [8]). Right: Flavor ratio probability distribution of astrophysical neutrinos above 35 TeV detected by IceCube [8].

of ultra-high energy cosmic rays detected from the Pierre Auger or the Telescope Array [11]. While there is no significant correlation with any class of extragalactic objects, the isotropicity of the neutrino flux strongly suggests the working assumption that it is of extragalactic origin.

2 Generic Source Requirements

A pre-condition for likely astrophysical VHE neutrino sources is that they also be sources of VHE cosmic rays, or else that they be irradiated by a flux of cosmic rays from some other source(s). So far, the isotropicity of the IceCube events has led to the search for possible candidates concentrating mainly in extragalactic space, e.g. [12]. Such sources could also be naturally related to the sources of ultra-high energy cosmic rays (UHECRs) observed by the Auger and TA cosmic ray arrays [11], although for the currently detected maximum neutrino energies of $\lesssim 3$ PeV it is only necessary to have sources capable of accelerating CRs up to $\lesssim 100$ PeV, as discussed below.

The spectrum shown in Fig. 1 can in principle be produced by a CR spectrum of roughly $N(E_p) \sim E_p^{-2.5}$, steeper than the -2 to -2.2 slope expected from first-order Fermi acceleration. The latter, if extending above ~ 100 PeV for the CRs would have resulted in a peak around 6.3 PeV in the electron antineutrino component due to the Glashow resonance, e.g. [13, 14, 15, 16, 17, 18, 19], a resonance which is so far not observed, IceCube detecting so far only upper limits above ~ 3.5 PeV. The options are either that

the diffuse spectrum is a single power law of slope ~ -2.5 , or else, if the spectrum is flatter below ~ 6.3 PeV, there could be a spectral break above a few PeV, which could arise naturally in some systems due to a steepening of the CR diffusion coefficient, e.g. [13, 20, 21, 22].

The Fermi diffuse isotropic gamma ray background in the $\sim 10 - 800$ GeV photon energy range imposes serious constraints on essentially all pp neutrino sources, and on most $p\gamma$ sources as well, because of the comparable fraction of π^0 production resulting in secondary TeV to PeV gamma rays which cascade against the infrared and microwave extragalactic background light (EBL), ending up down in the Fermi range, e.g. Fig. 2.

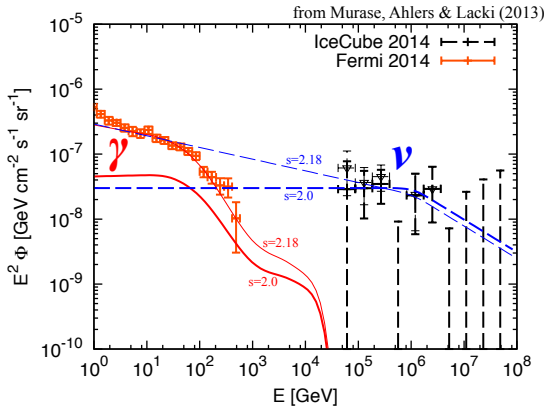


Figure 2: The isotropic gamma-ray background observed by Fermi compared to the diffuse per-flavor neutrino flux observed by IceCube. Black lines: possible neutrino models consistent with IceCube data. Red lines: the corresponding γ -rays of pp scenarios reprocessed in the external background light (EBL). The thick and thin solid lines show a power-law with slope $s = 2.18$ and $s = 2.0$, resp., with an exponential cutoff around PeV. From [23]; see also [24].

The secondary γ -rays have at birth the same slope as the neutrinos, and the branching ratio of charged to neutral pions in pp (or $p\gamma$) interactions implies that the two flux levels are related through $E_\gamma^2 \Phi_{E_\gamma} = 2E_\nu^2 \Phi_{E_\nu}$. These initial γ -rays of energy $E_\gamma \gtrsim m_e^2/E_{EBL}$ pair-produce against lower energy (infrared) photons from the diffuse EBL due to stars, as well as the cosmic microwave background. The pairs then inverse-Compton scatter against the same low energy photons resulting in new, lower energy γ -rays, etc. The resulting electromagnetic (EM) cascades lead to a universal spectral shape [25] which converts all the high energy γ -rays into lower energy, sub-TeV photons. *Fermi* is sensitive in the $\sim 0.1 - 800$ GeV range [26], and this provides strong constraints on models, and in particular on a hadronuclear origin of the neutrinos from any kind of sources, e.g. [13, 27, 21, 28, 22, 29, 30, 23, 24], see Fig. 2.

A dominant fraction of the Fermi diffuse extragalactic gamma background is in fact well accounted for by unresolved distant blazars [26], whose gamma-ray emission is most likely of leptonic origin, i.e. mechanisms which are not associated with neutrinos. On the other hand, many of the most commonly considered sources such as active galactic nuclei (AGNs), standard gamma-ray bursts (GRBs), etc. would be optically thin, i.e. allow free escape to both neutrinos and γ -rays, the latter being restricted by the Fermi observations. This restriction would not apply, however, to EM-“hidden” sources, e.g. [31], in which the $p\gamma$ or pp gamma rays are either absorbed or degraded to substantially lower energies, such sources being less (or not at all) constrained by Fermi.

For sources dominated by pp the efficiency (or optical depth) $\tau_{\gamma\gamma}$ of $\gamma\gamma$ absorption is generally uncorrelated to its pp pion formation efficiency f_{pp} , since the first depends on the photon target column density and the second on the proton target column density. For $p\gamma$ sources, however, there is a generic correlation [32] between $\tau_{\gamma\gamma}$ and $f_{p\gamma}$, since both depend on the photon target column density. The $p\gamma$ opacity is $\kappa_p\sigma_{p\gamma} \sim 0.7 \times 10^{-28} \text{ cm}^2$, where κ_p is the inelasticity, while the $\gamma\gamma$ opacity is $\sigma_{\gamma\gamma} \sim 0.1\sigma_T$, where σ_T is the Thomson cross section, so, e.g. [31], $\tau_{\gamma\gamma} \sim \sigma_{\gamma\gamma}/(\kappa_p\sigma_{p\gamma})f_{p\gamma} \sim 10^3 f_{p\gamma}$. Thus, for moderately efficient $p\gamma$ sources, the high energy γ -rays will be efficiently degraded. The final energy where they reappear after the cascades depends on the target photon energy spectrum. In addition, since the $\gamma\gamma$ cross section is close to that of Compton scattering, the photons can be trapped and partially thermalize as they diffuse out. This is important for sources such as AGNs, standard GRBs or others which are detected also in the optical, X-ray or MeV range, where additional constraints are imposed by stacking analyses of source locations against the error boxes of individual detected neutrinos. Thus, in general, compact high energy sources such as GRBs, especially choked GRBs [33, 34], white dwarf mergers [35], tidal disruption events [36, 37], core AGN sources [38], etc., by virtue of their high photon density are likelier to suffer photon trapping and efficient $\gamma\gamma$ degradation, making them EM-dim or effectively EM-hidden. As discussed in §3.1, another way in which ν, γ sources can be EM-hidden in the Fermi range is if they are at high redshifts $z \gtrsim 3-4$ [39, 40], the longer pathlength ensuring more efficient absorption in the EBL.

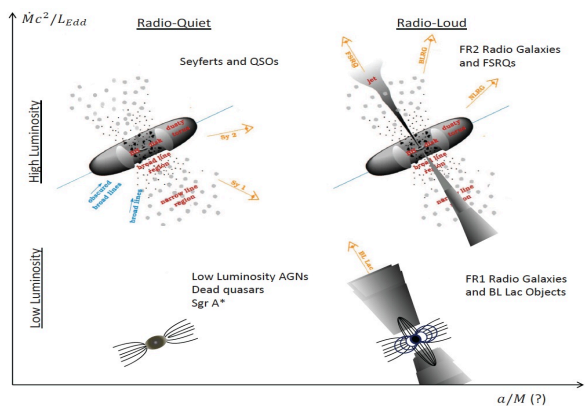
3 Specific Astrophysical Sources

3.1 Active galactic nuclei (AGNs)

The term AGN is applied to a small fraction of all galaxies in which either the galactic nucleus is a prominent source of radio or X-ray photons, or else (or in addition) it has bright jets emanating from the nucleus, which are detectable in radio, optical, X-rays or γ -rays. These emissions are powered by accretion onto a central massive black hole (MBH) in the nucleus. Average galaxies such as the Milky Way generally also have MBHs at the center, and in about $\sim 30\%$ of these the gas accreting into the MBH leads to detectable radio or X-ray emission, in the range of $10^{43} \text{ erg s}^{-1}$, these being called *low luminosity AGNs* (LLAGN). AGNs can have luminosities up to 4-5 orders of magnitude higher than LLAGNs, and are sub-divided into radio-quiet or RQ AGNs (a misleading term, since they have a dominant radio or X-ray nuclear emission, present also in LLAGNs); and radio loud or RL AGNs, which show luminous jets, detected mostly in radio but in some cases also in optical, X- and/or gamma-rays. The RQ and the RL AGNs represent roughly 10^{-1} and 10^{-2} of the total galaxy population. The RL (jet) AGNs are further sub-divided into the so-called FR-I and FR-II types. The FR-I have irregularly shaped, lower luminosity outer jets extending not far beyond the host galaxy, the nearest ones sometimes showing a bright, much straighter inner jet inside

the galaxy image². The FR-II have very extended, high luminosity narrow jets, whose dimension (up to few hundred Kpc) can far exceed that of the optical host galaxy.

Blazars are a rare sub-class of radio-loud AGNs ($\sim 10^{-5}$ of all galaxies), whose jets point close to the line of sight. The jets are relativistic (bulk Lorentz factors $\Gamma_j \sim 5 - 30$), implying a large Doppler boost of the jet luminosity, which dominates that of the host galaxy and the nucleus. Blazars include aligned FR-I AGNs called *BL Lac* objects, whose luminosities are not overly large, $\sim 10^{44} - 10^{45}$ erg s⁻¹; and aligned FR-II AGNs called *flat spectrum radio quasars* (FSRQs)³ whose luminosity is much larger, $\lesssim 10^{46} - 10^{47}$ erg s⁻¹ (Fig. 3.1).



Sketch of AGN types with relative radio-loudness in the X-axis and luminosity in the Y-axis, with an arbitrary division at 10^{45} erg s⁻¹ between LL AGNs and high luminosity (HL) AGNs, e.g. [41]. Clockwise from lower left (LL, RQ) one has LL AGNs, dead quasars, and our own galactic center radio source Sgr A*; top left (HL, RQ) are Seyfert galaxies and QSOs; top right (RL, HL) are FSRQs and FR2 Radio Galaxies; and bottom right (RL, LL) are Blazars and FR1 Radio Galaxies. From [41].

Models can generically be classified as leptonic, hadronic or lepto-hadronic type, depending on how important is the electromagnetic emission of the hadronic secondaries for the observed photon spectra. In leptonic models it is the primary accelerated electrons which are responsible for the photon spectra, even if hadrons were accelerated (their secondary EM emission is negligible). In hadronic models the hadronic secondary EM emission (or in some cases proton synchrotron) provides the bulk of the observed EM spectra, while in lepto-hadronic models it is a mix of both. Protons may be accelerated in all three types, and the CR efficiency is generally parameterized with the ratio of the luminosities in CRs and photons⁴, $\xi_{CR} = L_{CR}/L_{rad}$

RL AGNs, especially blazars, were the earliest suspected cosmic ray accelerator candidates. Their relativistic jets undergo strong shocks as they plow into the intergalactic medium, made detectable by the intense non-thermal radiation ascribed to synchrotron and inverse Compton from relativistic electrons, which are presumed to be accelerated into a power law distribution by a Fermi process in the high Mach number shocks. These termination shocks, as well as internal shocks closer in within the jet, are also ideal sites

²An example being the radio, optical and X-ray jets of the famous nearby M87 galaxy.

³Quasars, or QSRs, are AGNs powered by the most massive MBHs, $10^8 - 10^{10} M_{\odot}$; they are called QSOs when detected only in optical, and QSRs when detected in radio.

⁴Some authors use a ratio of CR luminosity to jet kinetic luminosity $\xi'_{CR} = L_{CR}/L_{kin}$.

for accelerating protons, and could be the source of the observed ultra-high high energy CRs (UHECRs) as well as high energy γ -rays, e.g. [42, 43]. An additional consequence of this would be VHE neutrinos, e.g. [44, 45]. This requires that the jet environment provide an adequate column density (or “optical depth”) of target photons and/or nucleons. Such targets are undoubtedly present, but the jets combine low target densities n_t competing with their large dimensions R in producing the optical depth $\tau_{pt} \sim n_t \sigma_{pt} R$ against proton or photon targets which make pions leading to ν, γ s, e.g. [46, 47].

In blazars there are four main sources of photons that act as targets for $p\gamma$ interactions, namely: 1) Continuum photons from the optically thick disk accretion disk which feeds the MBH, typically ranging over $\sim [10 - 10^5]$ eV; 2) Continuum infrared photons from a dusty torus, which often is detected outside the accretion disk, typically peaking around $\sim 10^{-2} - 10^{-1}$ eV; 3) Line ($H\alpha \sim 10$ eV) photons from the so-called broad line region (BLR) gas clouds detected outside the jet, especially in FSRQs; the BLR also scatters disk and torus continuum photons towards the jet, 4) Nonthermal emission from the inner jet, which in the so-called high-synchrotron peaked (HBL) BL-Lacs, which can be detected up to TeV photon energies, is a two-humped spectrum ascribed to synchrotron and synchrotron self-Compton (SSC); while in the low-synchrotron peaked (LBL) BL Lacs and FSRQs the two-humps are best fitted with jet synchrotron accounting for the low energy peak and external Compton accounting for the higher peak, i.e. scattering by jet electrons of “external” photons coming from either the accretion disk, the dust torus or, in FSRQs, the BLR’s own $H\alpha$ line photons plus the continuum disk and torus photons which it scatters into the jet.

Besides blazars, other types of AGNs may also contribute to the neutrino background, including radio-quiet quasars, e.g. [44, 48, 49] and LLAGNs [38]. The CR acceleration and neutrino emission of such RQ and LLAGN models is concentrated in the nucleus, where densities are larger. Since $\sigma_{pp} \sim 3 \times 10^{-26}$ cm² while $\sigma_{p\gamma} \sim 10^{28}$ cm² near threshold, while the relative increase of the nucleon density is larger than that of the photons, the pp interactions can become more important or even dominant.

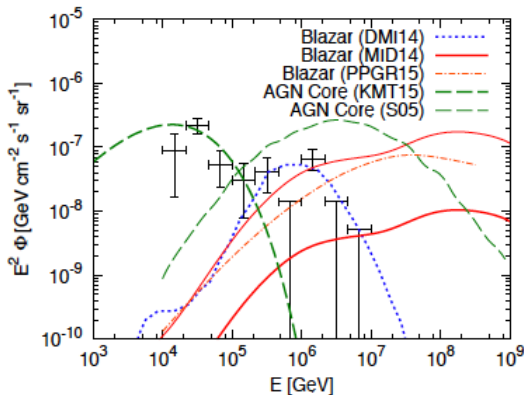


Figure 4: All-flavor diffuse neutrino intensity for various AGN jet and core models [50]: DMI14, a FSRQ jet model normalized to the IceCube data at PeV energies assuming $\langle z \rangle = 2$ [51]; MID14, two different leptonic blazar jet models with high/low CR efficiency [46]; PPGR15, a BL Lac jet model based on a lepto-hadronic scenario [52]; KMT15, a LLAGN core model [38]; S05, a radio-quiet AGN core model [53]. The diffuse neutrino intensity data is from the IceCube combined likelihood analysis [8].

Fig. 4 shows [50] a comparison of the diffuse neutrino background predictions from

some of the AGN models against IceCube data [8]. Typical blazar models have hard spectra, because the $p\gamma$ efficiency increases linearly with energy, and for a proton slope like -2 or -2.5 the neutrino spectrum has a positive slope. These models can explain the PeV data but under-predict the TeV data. Also, these models are in tension with the non-observation of a Glashow resonance at 6.3 GeV. The exception is a FSRQ model [51] where protons are accelerated by a Fermi 2nd order mechanism and the maximum proton energy at which acceleration balances escape is ~ 10 -100 PeV, while the main targets are BLR line photons of ~ 10 eV, giving a neutrino cutoff in the few PeV range. Older AGN core models have similar problems with the Glashow resonance and also under-predict the TeV data. A more recent LLAGN core model [38], assuming a radiatively inefficient accretion flow (RIAF) in which pp interactions dominate, reproduces well the 10-100 TeV data, but under-predicts the PeV data. These are typically one-zone models, which involve large astrophysical uncertainties, so although they all appear to have difficulties in fitting the spectral data they may not necessarily be ruled out. Other, weaker AGNs that have been considered are radio galaxies, e.g. [54, 55].

An important observational constraint is provided by a recent IceCube study [56] based on stacking analyses of spatial correlations, which sets limits on the possible cumulative contribution of Fermi-2LAC blazars to the diffuse TeV-PeV neutrino flux. They concluded that, assuming a -2.5 power law index, they can contribute at most 27%, or for a -2 index at most 50% of the total observed 10 TeV to 2 PeV neutrino flux, assuming complete oscillation between flavors. Similar results are obtained by [57]⁵.

3.2 Galaxy clusters/groups and associated sources and shocks

The importance of clusters of galaxies as amplifiers of the secondary radiation (neutrinos and gamma-rays) from intra-cluster UHECR sources was emphasized by [59, 60] and others. This is because the CRs, after having been accelerated and undergone some secondary-producing $p\gamma$ or pp interactions inside their immediate source of origin (AGNs, supernovae, etc.), they escape into the intra-cluster medium, which for large clusters of radius $R_{cl} \sim$ few Mpc has typically an average gas density $n_0 \sim 10^{-3} \text{ cm}^{-3}$, magnetic field strength $B_0 \sim 10^{-6} \text{ G}$ and coherence length $\ell_{coh} \sim 30 \text{ kpc}$. The typical diffusion coefficient $D(E_p) \propto E_p^\alpha$, where $\alpha = (5/3, 1/2)$ for Komolgoroff or Kraichnan turbulence spectra, and the diffusion time out of the cluster $t_{esc} \sim R_{cl}^2/6D$ exceeds by orders of magnitude the light crossing time $R_{cl}/c \sim 10 \text{ Myr}$. During this CR diffusion time their secondary-producing interactions exceed by far those undergone in their original source. The interactions after the CRs escape into the intergalactic medium (IGM) are typically less important than those undergone within a large cluster.

Accretion of external intergalactic gas onto the cluster gives rise to a stand-off shock, resulting in a shocked cluster gas layer and a stationary shock front facing the IGM. Such shocks can accelerate electrons to Lorentz factors $\gamma_e \sim 10^7$ which, as they scatter

⁵Noting that [58] argue that at a 3.3σ level a bright (HBL) sub-class of blazars could be responsible for some of the IceCube neutrinos as well as UHECRs.

off microwave background photons, can contribute [61, 62] to the diffuse extragalactic gamma-ray background. Cluster accretion shocks are also expected to accelerate CR protons, e.g. [63, 64], which undergoing photohadronic or hadronuclear interactions also contribute to the gamma-ray background, as well as to a diffuse neutrino background [65, 13, 30]. However, such cluster accretion shocks are in tension with clustering limits [12] and with radio limits [66].

Galaxy-galaxy collisions are also expected to occur in clusters of all sizes, all galaxies being thought to have undergone at least one (and for large galaxies many) major mergers in their history, in typical hierarchical growth structure formation schemes, e.g. [67]. Single galaxies move in the cluster with virial velocities, and shock-heat the intra-cluster gas, and also the gas in the colliding galaxy pairs undergoes strong shocks. The kinetic energy input rate is comparable to that of the accretion shock onto the cluster [68].

Fermi acceleration in these various types of shocks can lead to a power law energy distribution of CRs which are trapped in the cluster for a diffusion time, the latter depending on the shocked layer width, magnetic field strength and type of turbulence. For any such sources, the clusters act as CR reservoirs [60, 69, 70], providing for a longer time during which they produce secondaries, mainly via pp interactions. This leads to a neutrino spectrum whose slope mimics that of the protons and, assuming a slope $s \sim 2 - 2.2$, whose diffuse energy flux per energy decade $E_\nu^2 \Phi_{E_\nu}$, e.g. [13, 68] is comparable to that of the first IceCube flux data in the sub-PeV to PeV range [2]. One possibility which is allowed by the above mentioned clustering and radio limits is if CR acceleration occurs in AGNs in clusters and smaller groups of galaxies which serve as CR reservoirs [12], the effective density being larger than for accretion shocks since the low mass clusters can make a larger contribution. However, in all cases of optically thin sources (such as the above) proton slopes steeper than ~ -2.1 would result in violating the Fermi limits (see, e.g. Fig. 2). Here the true diffuse isotropic gamma-ray background is to be understood as the fraction remaining after subtraction of the resolved individual sources and the extrapolated contribution of unresolved sources [71].

The contributions to the diffuse secondary ν, γ backgrounds from all models will be lower [70] if the accelerated UHECRs are predominantly heavy elements, as suggested by the *Auger* observations [72, 73] at energies above $\sim 10^{18}$ eV. This is because the individual protons undergoing $p\gamma$ interactions carry only a fraction $1/Z$ of the total CR energy, while heavier nuclei are subject to photodesintegration, e.g. [74].

3.3 Starburst galaxies, supernovae and hypernovae

Starburst galaxies (SBGs) are normal galaxies which are undergoing episodes of intense star formation, $\dot{M}_* \sim 1 - 10 M_\odot \text{yr}^{-1}$, lasting $10^6 - 10^7 \text{yr}$, longer than the lifetime of young massive stars, which then become supernovae (SNe). Normal galaxies typically undergo a number of star-forming episodes since birth, and the steady-state density of galaxies which at any time are starbursts is $n_{SBG} \sim 3 \times 10^{-5} \text{Mpc}^{-3}$, roughly two orders of magnitude less than quiescent galaxies. About 20-30% of all star formation in the

Universe occurred in such SBGs.

Large numbers of SBGs with known redshift distances have measured radio luminosities at 1.4 GHz, which is due to synchrotron radiation by relativistic electrons whose cooling time is shorter than the SBG phase lifetime. Thus, the energy production rate of electrons is a measure of the radio luminosity L_ω per unit frequency ω , $E_e^2 dN_e/dE_e \simeq 2\omega L_\omega$, where the factor 2 arises because the synchrotron frequency $\omega \propto E_e^2$. In quiescent galaxies like ours the ratio of energy input in CR protons to electrons is $\eta_{p/e} \sim 50$, but as pointed out by [75], in SBGs the increased SN activity and a magnetic field $\gtrsim 10^2$ times larger than ours is likely to result in a much slower diffusive escape of the CR protons, which can lose most of their energy in pp interactions, leading to pions. The luminosity per decade of $\nu_\mu + \bar{\nu}_\mu$ is related to the photon luminosity ωL_ω by $E_\nu dL_\nu = (1/3)\eta_{p/e} E_e^2 d\dot{N}/dE_e = (2/3)\eta_{p/e}\omega L_\omega$, where the factor 1/3 is because 2/3 of the proton energy is carried by charged pions (1/3 by neutral pions), and since the charged pions decay into four particles ($\pi^+ \rightarrow \mu^+, \bar{\nu}_\mu \rightarrow e^+, \nu_e, \nu_\mu, \bar{\nu}_\mu$), about 1/2 of the charged pions's energy is carried by muon neutrinos. Also, since the secondary electrons carry $\sim (2/3) \times 1/4 \sim 1/6$ of the proton energy, in SBGs one expects a CR proton to electron ratio $\eta_{p/e} \sim 1/6$, so the muon neutrino luminosity per decade of energy is related to the photon luminosity per decade of frequency by $E_\nu dL/dE_\nu \simeq 4\omega L_\omega$, or $E_\nu^2(d\dot{N}/dE_\nu) \simeq 4E_\gamma^2(d\dot{N}/dE_\gamma)$. Thus, one can calibrate the CR luminosities of SBGs, or their expected neutrino energy flux, via their observed 1.4 GHz radio luminosities. A similar calibration can be also based on an established correlation of the infrared luminosity to star-formation rate in SBGs. By analogy with our galaxy's observed CR spectrum below the knee of $N_{obs}(E_p) \propto E^{-2.75}$ and its confinement time $t_{esc} \propto E^{-0.6}$, [75] assume a similar inferred injection spectrum $N(E_p) \propto E^{-2.15}$ for the SBGs. This predicts a well-motivated SBG neutrino diffuse flux, shown in fig. 5, which is comparable to the Waxman-Bahcall (WB) flux [76]. A flux of that order is indeed being observed by IceCube [2, 3], although there is so far no direct evidence linking it to SBGs.

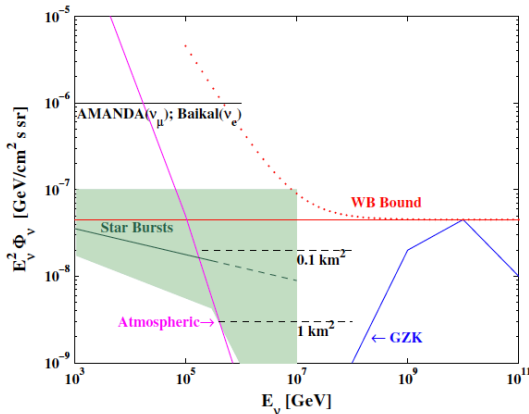


Figure 5: The possible starburst neutrino background (shaded). The upper boundary is for a CR index $s = 2$, lower boundary is for $s = 2.25$ for $E_\nu < 10^{14.5}$ eV. The solid green line is for $s = 2.15$. Also shown: the WB upper bound; the neutrino intensity expected from interaction with CMB photons (GZK); the atmospheric neutrino background; some experimental upper bounds @ 2006, and the approximate sensitivity of 0.1 km² and 1 km² optical Cherenkov detectors. From [75].

Supernovae are the most likely ultimate sources responsible for accelerating the CRs in SBGs, which make many more SNe during their starburst phase than normal galaxies.

A sub-class of supernovae, called hypernovae (HNe), representing a fraction $\sim 5\%$ of the total, are known to occur in all galaxies. Their ejecta velocities can reach semi-relativistic values, as opposed to $v_{ej} \sim 10^9 \text{ cm s}^{-1}$ for normal SNe, and their ejecta kinetic energies (isotropic-equivalent value) can reach $\sim 10^{52} \text{ erg}$, as opposed to $\sim 10^{50} - 10^{51} \text{ erg}$ for SNe. The maximum CR energy achievable by Fermi shock acceleration, from eq. (9), is $E_{max} \gtrsim 10^{15} Z eV$ for SNe and $E_{max} \sim 10^{17} Z \text{ eV}$ for HNe. This was used [77, 78] for making source-specific neutrino background predictions before IceCube observations were available, and subsequently, in the light of both IceCube and Fermi data, hypernova neutrino production were discussed e.g. by [20, 21, 79, 28, 80]. A more detailed discussion of the neutrino production and the constraints imposed by Fermi was given by [22] for both supernovae and hypernovae in SBGs and star-forming galaxies, including the proton diffusion time in the host galaxy and host cluster while undergoing pp interactions. These results indicated that SNe and HNe within redshifts $z \lesssim 4$ could at most provide a fraction 0.2-0.3 of the neutrino background without overproducing the observed gamma-ray background. However, there are uncertainties in the star-formation rate at $z \gtrsim 2$, e.g. [81], as well as in the ratio of HNe to SNe, both of which get worse at higher redshifts. On the other hand, as shown by [39], the γ -rays from sources at redshifts $\gtrsim 3$ undergo increasingly severe degradation due to a rise in the $\gamma\gamma$ interactions in the increasingly dense intergalactic photon bath. Thus, the constraints from the Fermi observations can be satisfied [40] when one considers a significant contribution of SNe and HNe at redshifts $4 \lesssim z \lesssim 10$ from the first generations of stars (the so-called Population III stars). Of course, the apparent surface density of galaxies at high redshifts gets very large, which makes it difficult to correlate any neutrino positions with candidate sources.

A discussion of the general conditions in SBGs and milder star-forming galaxies, including star formation rate, gas densities, magnetic fields and dimensions was given by [82]. Note that the starburst phenomenon is also suspected, in some cases, to have been initiated by a merger of two galaxies, in which case large scale shocks would arise which, as discussed in §3.2, leading to CR acceleration and secondary neutrinos and γ -rays. There are also systems in which an AGN and a starburst co-exist, and based on SBG luminosity functions these could also be relevant for the neutrino background. Of course, starburst galaxy systems are also subjected to the Fermi-imposed restriction requiring effective CR slopes flatter than ~ -2.2 , e.g. [13, 12].

3.4 Gamma-Ray Bursts

The so-called “classical” GRBs have long been considered as likely candidates for high energy neutrino production [32]. GRBs are catastrophic stellar events brought about by the core collapse of a massive star or the merger of a compact degenerate binary, leading to the most energetic explosions in the Universe. These result in highly relativistic jets which emerge from the collapsing or merging progenitor system, with bulk Lorentz factors $\Gamma \sim 10^2 - 10^3$. In the case of the core-collapse events (“long” GRBs, with MeV γ -rays lasting over 2 s) sometimes an accompanying type Ic supernova is also detected,

in which the progenitor star’s envelope is ejected⁶. GRBs are detected when spacecraft such as Swift or Fermi trigger on an initial prompt γ -ray burst lasting milliseconds to tens of minutes, over the range of $\sim 0.1 - 10$ MeV, and sometimes up to ~ 100 GeV, e.g. [83, 84]. The prompt emission is generally followed by a slowly decaying afterglow which ranges from X-rays through optical down to radio, over days to months. The photon spectra of both the prompt and afterglow emission look non-thermal, and have been generally ascribed, e.g. [84], to electron synchrotron and inverse Compton. The prompt emission is typically modeled with Fermi acceleration in internal shocks inside the jet, while the afterglow arises from acceleration in an external shock, where the jets plows into the external medium. For the prompt emission, besides internal shocks, other alternative mechanisms for the nonthermal emission have also been proposed, including emission following reconnection or hadronic dissipation at a scattering photosphere, or emission from an intermediate zone due to shocks and magnetic reconnection or hadronic dissipation and reacceleration, e.g. [85, 86, 87, 88, 89]. The acceleration of protons is expected to lead, via $p\gamma$ interactions in internal shocks, to TeV energy neutrinos [32], and in external shocks to EeV energy neutrinos [90]. GeV neutrinos are also expected from proton acceleration and pp or $p\gamma$ interactions in photospheres [91, 92, 93, 94], and up to multi-TeV can be produced in intermediate magnetic or hadronic dissipation zones [89, 95, 96].

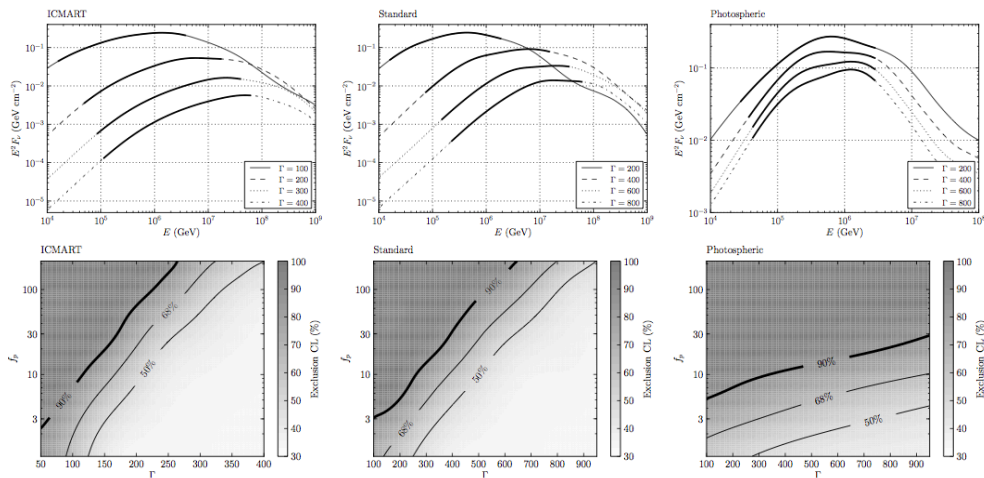


Figure 6: Top: Total normalized neutrino fluxes for ICMART, IS and (baryonic) photosphere models (left to right) for various Lorentz factors Γ , scaling with f_p (which here is 10). Bottom: Allowed region for f_p and Γ for the different models. From [97].

The initial IceCube tests of GRB neutrino models derived upper limits from the initial 40 string and 52 string arrays [98, 99, 100] by comparing against a simplified internal shock (IS) model with an unchanging radius parameterized by the total γ -ray energy, Lorentz factor Γ , outflow time variability t_v and a standardized broken

⁶However, only a very small fraction of all SN Ic are associated with GRBs.

power law photon spectrum, using the Δ -resonance approximation for the photohadronic interaction, and assuming a CR baryon loading (relativistic proton to electron ratio) $f_p = L_p/L_e$. This initial study concluded that for $f_p = f_e^{-1} = L_p/L_e = 10$ this model over-predicted the data by a factor 5, and a model-independent analysis comparing the observed diffuse neutrino flux to that expected also gave negative results. This was an important first result from IceCube, demonstrating the ability of a major new Cherenkov neutrino facility to test astrophysical models. Subsequently, using the same IS model but correcting various approximations and including also multi-pion and Kaon channels as well as interactions with the entire target photon spectrum [101, 102, 103], lower model fluxes were calculated which did not disagree with the 40+56 string data. Interestingly, the original approximate IS calculation of [32] had also resulted in a lower flux which is a factor 10 below the WB bound, and within the above IceCube limit.

Much more extensive tests of GRB prompt emission models were made against a set of more accurate internal shock models, as well as a magnetic dissipation model (ICMART) [88] and a baryonic photospheric model [92, 96], assuming a steady state, fixed radius emission zones. These statistical tests were made against four years of IceCube data, including two years of the full array [97]. They concluded (Fig. 6) that at 99% confidence level less than 1% of the observed diffuse neutrino background can be contributed by the observed sample of 592 EM-detected GRBs. If the basic acceleration paradigm used for the emission zones is correct, and this result continues to stand, it would be indicating that the ratio $f_p = L_p/L_e \lesssim 1$ in such models. Other photospheric models with substantially different neutrino production physics [93, 104] or including time-dependence [95] have been calculated which may avoid these restrictions, but these have so far been only qualitatively compared against the data.

The classical GRBs discussed above are typically bright, and are EM-detected by spacecraft at an observed rate of $\sim 300\text{yr}^{-1}$, or $\sim 700\text{yr}^{-1}$ when corrected for viewing constraints, the total sample measuring in the thousands. There are, however, other known or suspected types of GRBs, as discussed next.

3.5 Low luminosity, shock-breakout, and choked GRBs

Low luminosity GRBs (LL GRBs) have been observed for a long time, although only a few are known so far, all of which were detected at very close distances $z \ll 1$ due to their intrinsic EM-dimness ⁷. LLGRBs appear to be a distinct class, although aside from their low luminosity they share many of the classical long GRB characteristics, e.g. a non-thermal, albeit softer, spectrum which may be related to a relativistic jet which emerged from a collapsing stellar progenitor. Being nearby, a supernova ejecta is generally detected as well, which appears to be semi-relativistic, e.g. [105, 106]. However, their local occurrence per unit volume rate is an order of magnitude higher than for classical GRBs, e.g. [107]. classical GRB IS model's neutrino luminosity suggests that LLGRBs could contribute significantly to the diffuse neutrino background [108, 109].

⁷Unlike classical, high luminosity GRBs, which have been detected in $0.5 \lesssim z \lesssim 9$ range.

Shock-breakout GRBs, of which even fewer have been detected, also show a soft low luminosity gamma-ray and/or X-ray burst, e.g. [106], followed by a brightening of the UV and later optical radiation which bears resemblance to a supernova brightening, but with distinct characteristics. It is thought that this phenomenon involves a jet emanating from the core of a collapsing massive star, as for classical long GRBs, but which had less momentum and just barely managed to break out from the star. As the jet propagated it imparted extra energy to the expanding stellar envelope, and the boosted supernova shock appears to break out (i.e. the photon diffusion time become shorter than the expansion time) in a dense wind which precedes the ejecta [110, 111].

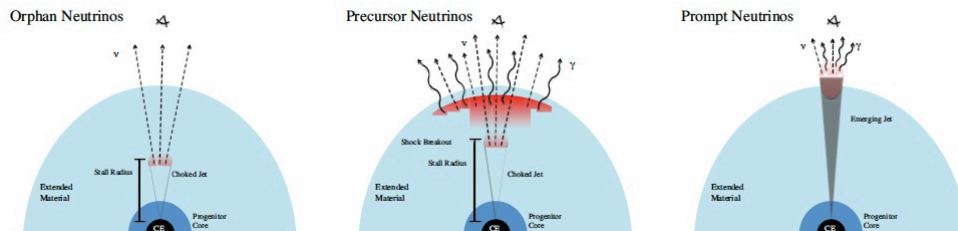


Figure 7: Sketch of possible scenarios for jet and stellar envelope interaction in a core collapse. Left: Choked jet and orphan neutrinos. Middle: precursor neutrinos and shock-breakout. Right: Low-luminosity emergent jet GRB. From [34].

Choked GRBs, which were posited [112] before shock-breakouts and extragalactic neutrinos were discovered, are core-collapse objects where the jets did not emerge, either because they did not have enough momentum, or because they were not powered long enough to reach the outer radius of the stellar envelope. Internal or recollimation shocks (or magnetic dissipation) in such stalled, buried jets could accelerate protons leading to GeV neutrinos, while the gamma-rays would be thermalized, and only a subsequent optical supernova would be expected, which at redshifts $z \gtrsim 1$ is rarely detectable. Searches with IceCube have so far not yielded candidates [?]. Alternatively, if the jet was energetic enough to eventually emerge, before doing so the pre-emergence jet could again undergo shocks or dissipation giving rise to a neutrino precursor, followed by a successful GRB, which could be an LLGRB or a classical GRB as opposed to a failed (choked) GRB [112]. The shock-breakouts represent an intermediate case between the choked and the emergent. A unified picture of the electromagnetic properties expected from all three cases was discussed by [114].

All three of these LL GRB types, see Fig. 7, would be expected to be “hidden ” neutrino sources, since their EM emission is either so weak that only the very few nearest cases trigger a γ -ray detector, or else their EM luminosity is a protracted supernova-like event in the optical/IR, and being typically at very high redshift it is again hard to detect. Both analytical and in some cases numerical calculations of the high energy neutrino spectral fluences were carried out separately for choked jets [115, 116, 117, 118, 119, 33, 120], shock-breakout GRBs [121, 122, 123] and LLGRBs [108, 124].

More recently, a unified calculation and comparison of all three types of hidden GRBs

(choked, break-out and low-luminosity) was carried out [34], see Fig. 8. This calculation used a standard GRB luminosity function, and neutrino emission was considered only from choked or precursor jets whose luminosity was low enough to ensure that the buried shocks are not radiation-broadened (since buried jets are at lower radii and their radiation density is comparatively higher than in emergent jets). This ensures a collisionless shock, in which that particles scattered between pre- and post-shock regions are subjected to the full bulk velocity difference, as needed for first-order Fermi acceleration. Otherwise, for higher luminosity buried jets, the photon mean-free path governs the shock width, which becomes larger than the typical photon mean-free path or gyro-radius, the scattered particles are not exposed to the full bulk velocity difference, and classical first-order Fermi acceleration is not expected, e.g. [125, 33]. Low-power jets are also required in order for the jet to stall before it emerges from the star [33, 34].

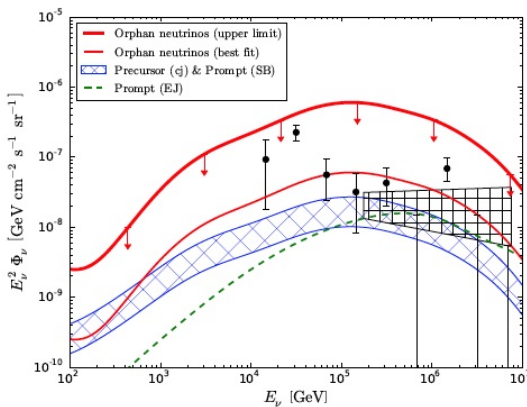


Figure 8: Predicted all-flavor diffuse neutrino fluxes from three types of low-luminosity GRBs: choked jets (orphan neutrinos, in red); precursor and shock-breakout neutrinos (blue); and prompt emergent jet LLGRB neutrinos (dashed). From [34].

The conclusion from this calculation [34] is that a combination of choked jet, shock-breakout and low-luminosity GRBs could in principle provide the observed IceCube neutrino flux, without violating either the Fermi observations nor the (classical GRB) stacked neutrino analyses.

3.6 Other sources: tidal disruptions, white dwarf mergers

Tidal disruption (TDE) events of stars by massive black holes at the centers of some galaxies can also lead, in a fraction of the cases, to relativistic jets, as in the gamma-ray source Sw J1644+57 [126]. It has also been proposed that TDEs could be accelerators of UHECRs [127]. If such tidal disruptions occur in a galactic whose bulge gas density is large enough, or if the tidal disruption initially leads to a precursor wind before the jet is produced, e.g. [128], this external gas may either choke the jet or it may lead to a shock-breakout similar to that in GRBs, e.g. [36]. The rates are highly uncertain, but a fraction of the observed VHE neutrinos may arise from such events, whose gamma-rays could be effectively EM-hidden because of the high optical depth of the enshrouding gas, some recent calculations being, e.g., [37, 129, 130].

White dwarf (WD) mergers are another possible type of hidden neutrino source. WDs are the remnants of most SN explosions, and WD binaries are abundant enough that their merger rate is estimated to be comparable to that of the SN Ia. Such WD mergers may lead to a magnetized outflow [131], in which photons are trapped up to the diffusion radius where the diffusion time is equal to the dynamic time. Magnetic reconnection in the flow beyond the diffusion radius can lead to proton acceleration which gives rise to pp interactions resulting in secondary neutrinos and gamma-rays [35]. Since the scattering optical depth is still large at the diffusion radius, the gamma-rays are degraded and these sources are effectively dark, or at least considerably dimmed, as far as the Fermi energy sensitivity range, thus avoiding the Fermi constraint. The neutrino flux can be a substantial fraction of the IceCube flux, depending on model uncertainties and WD merger rates.

There are other stellar sources in starburst galaxies which have been considered for producing very high energy neutrinos, including magnetars, young pulsars and macro-novae, which cannot be covered here.

4 Discussion

The discovery of extragalactic very high energy neutrinos by IceCube has opened an entirely new realm of possibilities for exploring the physics of the highest energy astrophysical sources, potentially out to the most distant reaches of the Universe. However, the small number of events at these energies allows one to address so far only the aggregate emission in the form of a diffuse background radiation. The identity and nature of the sources remains unknown, although it is realistic to expect significant progress in this respect with multi-messenger approaches, such as the AMON project [132, 133] and others, especially those involving neutrino detections combined with the (relatively) more easily detectable electromagnetic counterparts.

With accumulating high energy neutrino and gamma-ray data it will become increasingly feasible to draw general conclusions about the physical mechanisms producing the neutrinos, as well as about the general environment in which they originate and in which their secondaries propagate, e.g. [8]. Furthermore, these neutrinos and their co-produced gamma-rays must be linked to high energy cosmic rays of energy in the $10^{14} - 10^{17}$ eV range, and possibly beyond. The fact that the IceCube neutrino emission level is close to the Waxman-Bahcall limit [76] has provided the motivation for an interesting argument [134] indicating that the input of cosmic ray energy per decade over their entire spectral range may be approximately constant at the level of $\sim 10^{44}$ erg Mpc $^{-3}$ yr $^{-1}$, whose manifestation in the IceCube range would be the observed neutrinos, e.g. [135, 12].

Further progress can be expected with the future completion of the KM3NeT underwater neutrino detector in the Mediterranean [136], with roughly similar capabilities as IceCube and a complementary northern hemisphere location. Both IceCube [137] and KM3NeT [136] have proposed extension proposals to their sensitivity to lower and higher energies, which could also address interesting questions of fundamental physics,

e.g. [138], and dark matter [139, 140]. Much larger effective area detectors, such as the ANITA balloon telescope, e.g. [141], the proposed very large radio arrays in Antarctica such as ARIANNA [142] and ARA [143], and space-based detectors such as JEM-EUSO [144], will extend the sensitivity to the very low fluxes expected at energies in the $10^{20} - 10^{21}$ eV range and above, which can address important questions of cosmogenic neutrino production, including testing for the presence of UHECR at or beyond the GZK radius ~ 100 Mpc, whether the spectrum extends beyond the GZK energy $\sim 6 \times 10^{19}$ eV, constraining the heavy element content, etc. The completion of the approved CTA (Cherenkov Telescope Array) large ground-based VHE gamma-ray detector, e.g. [145], will also be extremely useful for simultaneous neutrino and gamma-ray detections, localizations and source characterizations.

MAIN SUMMARY POINTS:

1. Extragalactic TeV-PeV neutrinos have been discovered, heralding a completely new channel for studying extreme high energy cosmic physical processes at the highest redshifts in the Universe.
2. These neutrinos carry important clues for investigating the origin of the high energy cosmic rays, and they provide stringent constraints for the possible source models being considered.
3. A smoking-gun identification of the actual sources remains so far elusive, since the angular accuracy of the arrival directions of individual neutrinos remains of the order of a degree or larger.
4. Co-emitted gamma-rays, when detected, are likely to help address this problem, as will also statistical analyses based on larger numbers of neutrinos and more complete candidate source catalogs.
5. We live in an exciting new era, where tremendous progress is being made.

FUTURE ISSUES

1. The main desiderata for future advances will be to achieve significantly higher event statistics, which requires, e.g., the approval and building of the Gen2 extensions to IceCube, the completion of new facilities such as KM3NeT, and the expansion of multi-messenger localization operations such as AMON.
2. The above sensitivity increases are also crucial for investigating pressing issues of basic neutrino physics, for dark matter searches, and other beyond-the-standard model questions.
3. A major current problem is that the observed diffuse neutrino background flux appears to over-predict the observed diffuse gamma-ray flux, assuming the ‘usual suspect’ optically-thin candidate sources.

4. Unless otherwise resolved, the above issue is suggestive of electromagnetically hidden sources, i.e. sources where gamma-rays are absorbed or degraded. Possibilities being considered are buried low-luminosity GRB jets or tidal disruption jets, among others, but much more work remains to be done.
5. Many new surprises can be expected from the major new facilities coming online in the next decade.

DISCLOSURE STATEMENT

The author is not aware of any affiliations, memberships, funding, or financial holdings that might be perceived as affecting the objectivity of this review.

ACKNOWLEDGMENTS

The author is grateful to Douglas Cowen, Kohta Murase and Marek Kowalski for useful communications. and to NASA NNX13AH50G for partial support.

5 Appendix

5.1 Neutrino Production Mechanisms

Aside from the possibility of high energy (\gtrsim GeV) neutrinos being produced by the decay of exotic (beyond the Standard Model) particles, the production of such neutrinos is expected in astrophysical scenarios. Cosmic rays can lead, via hadronic interactions such as pp , pn or $p\gamma$ to the production of mesons, mainly π^\pm , π^0 , which decay as, e.g., $\pi^+ \rightarrow \mu^+ \nu_\mu$ followed by $\mu^+ \rightarrow e^+ \nu_e \bar{\nu}_\mu$ or $\pi^0 \rightarrow 2\gamma$. For proton (or neutron) CRs the energy of the decay neutrinos is typically related to the parent cosmic ray p or n energy by $\varepsilon_\nu \simeq 0.04 - 0.05 \varepsilon_{p,n}$. For a total cosmic ray (proton) volumetric energy generation rate Q_p [erg Gpc $^{-3}$ yr $^{-1}$] leading to a CR energy generation rate per decade of energy $\varepsilon_p Q_{\varepsilon_p}$, one expects an all-flavor neutrino energy generation rate per decade of energy of

$$\varepsilon_\nu Q_{\varepsilon_\nu} \approx \frac{K}{(1+K)} \left(\frac{3}{4}\right) \min[1, f_{p\gamma/pp}] \varepsilon_p Q_{\varepsilon_p}, \quad (1)$$

where by ε_j we denote the source-frame energy of particles of type j . Here the (3/4) factor enters because roughly 1/4 of the energy in the decay chain is lost to e^\pm which end going into photons, and K is the average number ratio of charged to neutral pions, which is $K \simeq 1$ for the $p\gamma$ and $K \simeq 2$ for pp, pn processes. The factor $\min[1, f_{p\gamma/pp}]$ is the pp or $p\gamma$ meson production efficiency,

$$f_{p\gamma/pp} \simeq n_{\gamma/p} \kappa_p \sigma_{p\gamma/pp}^{incl} c t_{int} \quad (2)$$

where $n_{\gamma/p}$ is the number density of target photons (protons), κ_p is the inelasticity (i.e. the relative energy loss per interaction, $\Delta\varepsilon_p/\varepsilon_p$), which on average is $\kappa_p \simeq 0.5$ for both pp and $p\gamma$, the inclusive (i.e. total) cross section is $\sigma_{p\gamma}^{incl} \simeq 5 \times 10^{-28} \text{ cm}^2$ for $p\gamma$, or $\sigma_{pp}^{incl} \simeq 8 \times 10^{-26} \text{ cm}^2$ for pp , and t_{int} is the time available for interactions, with ct_{int} the interaction length. The interaction time is generally $t_{int} = \min[t_{inj}, t_{esc}, t_H]$, where t_{inj} is the CR injection time, t_{esc} is the CR escape time from the interaction region, t_H is the local Hubble time or age of the Universe in the source frame, and the interaction length is along a random walk path between interactions.

The neutral pions result in an accompanying gamma-ray emission, $\pi^0 \rightarrow 2\gamma$, which is related (at the source) to the neutrino emission by

$$\varepsilon_\gamma Q_{\varepsilon_\gamma} \approx \frac{1}{K} \frac{4}{3} \left(\varepsilon_p Q_{\varepsilon_p} \right) |_{\varepsilon_\nu = \varepsilon_\gamma/2} \quad (3)$$

where the energy of the γ -rays are, on average, $\varepsilon_\gamma \simeq 2\varepsilon_\nu$.

Denoting with E_j the energies of particles j observed at Earth, the neutrinos observed by IceCube from a source at redshift z are related to the parent proton energy by

$$E_\nu \sim 0.05 E_p \simeq 2 \text{ PeV } \varepsilon_{p.17} [2/(1+z)], \quad (4)$$

and the all-flavor diffuse neutrino flux Φ_ν per steradian with observed energy E_ν at Earth is

$$E_\nu^2 \Phi_\nu = \frac{c}{4\pi} \int \frac{dz}{(1+z)^2 H(z)} [\varepsilon_\nu Q_\nu] |_{\varepsilon_\nu = (1+z)E_\nu}, \quad (5)$$

in units of, e.g. $\text{GeV cm}^{-2} \text{ s}^{-1} \text{ sr}^{-1}$. Here $H(z) \simeq H_0 [\Omega_V + (1+z)^3 \Omega_M]^{1/2}$ is the redshift-dependent Hubble parameter, with $H_0 \simeq 70 \text{ Km/s/Mpc}$.

For a local ($z = 0$) CR proton differential energy input rate Q_{E_p} , the diffuse neutrino background *per flavor* at Earth which follows from eq.(5) is approximately

$$E_\nu^2 \Phi_\nu \approx \frac{ct_H \xi_z}{4\pi} \left[\frac{K}{4(1+K)} \right] \min[1, f_{p\gamma/pp}] (E_p Q_{E_p}), \quad (6)$$

e.g. [32, 13], where the per-flavor factor is $[K/4(1+K)] = [1/8, 1/6]$. i.e. $1/8$ for $p\gamma$ ($K = 1$) or $1/6$ for pp ($K = 2$), $t_H \simeq 13.2 \text{ Gyr}$, and ξ_z is a redshift evolution factor, which, e.g. for sources evolving approximately as the star-formation rate, such as GRBs or SNe, is $\xi_z \sim 3$ at $z \sim 1$. The corresponding diffuse γ -ray background associated with eq.(6), in the absence of electromagnetic (EM) cascades, is given by

$$E_\gamma^2 \Phi_\gamma \approx 2 \left(E_\nu^2 \Phi_\nu \right) |_{E_\nu = 0.5 E_\gamma} \quad (7)$$

5.2 Cosmic Ray Acceleration Mechanisms

The photons or hadrons entering the $p\gamma$ or pp , pn , etc. interactions must have energies such that the center of momentum (CM) energy is above threshold for producing pions or

other mesons. Thus either the photons involved in $p\gamma$ must have high lab-frame energies, or the hadrons initiating the pp or $p\gamma$ interactions must be highly relativistic, i.e. they must be cosmic rays (CRs). Among the most promising mechanisms for CR acceleration are the diffusive shock acceleration (DSA) and magnetic reconnection acceleration, both of which are first-order Fermi type mechanisms; stochastic or turbulent acceleration, which is a second-order Fermi type; and electrostatic type acceleration mechanisms, such as pulsar magnetospheric acceleration, or wake field acceleration.

The DSA mechanism can arise in systems where a strong shock propagates, with charged particles scattering back and forth across the shock interface. Typically such shocks are collisionless, i.e. the binary particle collision mean-free-path is very large compared to that for scattering by magnetic irregularities. For a sub-relativistic (or mildly relativistic) shock propagating into a stationary upstream medium, a proton which is already relativistic in the downstream (moving) region can run ahead of the shock, and will be randomized by scattering against magnetic irregularities in the upstream region. The particle is then overtaken by the shock, finding itself again in the downstream region where it is again randomized again by magnetic irregularities. The process then repeats itself, and at each step of the cycle the particle gains energy at the expense of the upstream-downstream gas relative bulk velocity difference. Each time the particle is hit head-on, the net relative energy boost being $\Delta E/E \propto (v_s/c)$ (hence first order), where v_s is the shock velocity⁸.

In such first order shock acceleration scenarios, the typical acceleration timescale is

$$t_{ac}^{dsa} \simeq \eta \left(\frac{r_L}{c} \right) \beta_s^{-2} \quad (8)$$

where $r_L = E/ZeB$ is the Larmor radius, Ze is particle charge, B is magnetic field and $\beta_s = v_s/c$ is the shock velocity in the upstream frame, and $\eta \sim 1 - 10$. This acceleration timescale is of the order of the gyration time, being proportional to the maximum particle energy ε reached, and is controlled by the *spatial* diffusion time. If the shocks occur in a jet oriented towards the observer with a bulk Lorentz factor Γ , the acceleration time, Larmor radius, magnetic field and shock velocity in eq.(8) should be read as the corresponding quantities in the jet frame, t'_{ac} , r'_L , B' and β'_s . A limit on the maximum energy is imposed by requiring that t_{ac} not exceed the dynamic time, $t_{dyn} \simeq R/v_s$ in the non-relativistic (NR) case, where R is the lab-frame dimension of the acceleration region (e.g. radius of shock),

$$E_{max} \simeq \left(\frac{\beta_s}{\eta} \right) \frac{ZeBR}{(1+z)}, \quad (9)$$

where z is the redshift of the source⁹. This criterion is equivalent to the confinement

⁸Two things to note: one is the initial particles injected must already be at least mildly relativistic; and for relativistic shocks, the treatment is more complicated after the first scattering, but under some approximations qualitatively similar results are expected.

⁹More exactly, if the minimum spatial diffusion coefficient in the Bohm limit is $D_{min} = \eta' r_L c / 3$, then $t_{ac}^{dsa} \simeq (20\eta'/3)(r_L/c)\beta_s^{-2}$, and $\varepsilon_{max} \simeq (3\beta_s/20\eta')ZeBR/(1+z)$

criterion that r_L be smaller than the acceleration region R . For shocks in a jet with bulk Lorentz factor Γ , in the comoving frame $t'_{dyn} \simeq R/c\Gamma$, so $(20\eta/3)(r'_L/c)\beta_s'^{-2} \leq (R/c\Gamma)$ leads to a lab-frame maximum energy given by eq.(9) but with β_s replaced by $\beta_s' \rightarrow 1$ and B replaced by B' , the comoving field. Alternatively, the maximum energy may be limited by the requirement that the acceleration time be shorter than the synchrotron radiation loss time of the accelerated particle.

Magnetic reconnection is another acceleration process which operates as a Fermi first order mechanism. Long considered as the cause of particle acceleration in solar flares, its occurrence is expected to be ubiquitous in many astrophysical situations where shear, turbulence or rotation lead to reconnection. Candidate sites include, besides flares, azimuthally sheared accretion disks, transverse shear between jets and environment, MHD turbulent media, etc. A schematic X-point geometry considers regions of dimension ℓ_{rec} of opposite magnetic polarity which approach each other, e.g. along the $\pm y$ direction, at a sub-relativistic speed $\beta_{rec} \lesssim 0.1$ leading to a thin reconnection layer with an electric field along the x -axis where plasma flows out along the $\pm x$ -axis at the Alfvén speed $V_A \sim 1$. Charged particles are caused to rotate repeatedly in and out of the opposite converging regions under the action of the opposite magnetic field polarities, while experiencing a net acceleration along the x -axis under the effect of the reconnection layer's electric field. A simple but illustrative calculation [146] shows that the effective acceleration timescale is $t_{ac}^{rec} \simeq (2\pi/[1-1/A])(r_L/c) \sim 4\pi(r_L/c)$, where for reasonable reconnection rates $A \sim 2$, giving an acceleration timescale which is essentially eq.(8) for the diffusive shock acceleration, i.e. roughly the gyration period. The maximum particle energy is again obtained by equating the acceleration time to the dynamic time, leading approximately to eq.(9), or by equating the acceleration time to the radiation loss time.

Stochastic acceleration, such as expected in MHD turbulent media as particles are scattered by waves of velocity v_w with random orientations, leads as mentioned to relative energy changes which are second order, $\propto (v_w/c)^2$, because the particles suffer both head-on and overtaking collisions with the waves. This is a process of diffusion in energy space, the particles sometimes gaining and sometimes losing energy, the first order energy changes canceling out, but resulting on a net average energy gain. For magnetic field fluctuations with a spectral energy density $W_k \propto k^{-q}$, where $k =$ wavenumber corresponding to turbulent lengthscales $\ell \sim 2\pi/k$, for resonant scattering (where $r_L \sim k$) one expects an energy diffusion coefficient $D_{\varepsilon\varepsilon} \propto \varepsilon^q$, and a scattering and acceleration time $t_{ac} \propto \varepsilon^{2-q}$,

$$t_{ac}^{sto} \simeq \frac{\varepsilon^2}{4D_{\varepsilon\varepsilon}} \sim \eta_{sto} \frac{\ell_t}{c} \left(\frac{r_L}{\ell_t} \right)^{2-q} \quad (10)$$

where $\ell_t \sim 2\pi/k_{min}$ and $\eta_{sto} \sim 1$, e.g. [147, 148, 149]. This timescale is generally longer than that of eq.(8) for shock acceleration, but is still shorter than the MHD wave timescale ℓ_t/c , so it can act as a slow-heating mechanism on a sub-hydrodynamical timescale [148, 89]. At the highest energies, where $r_L \sim \ell_t$, or for values of $q = 2$ as suggested by various MHD turbulence simulations, the energy diffusion coefficient becomes $D_{\varepsilon\varepsilon} \propto \varepsilon^2$ [150], and the stochastic timescale becomes comparable to eq.(8)

for shock acceleration. Equating the acceleration time (10) to the hydrodynamic time $R/c\beta\Gamma$ (or $R/u = R/c\beta$ in the non-relativistic case) the lab-frame maximum energy is

$$E_{max} \simeq ZeB\ell_t \times \begin{cases} 1 & \text{for } q = 2 ; \\ (R/\eta\beta\Gamma\ell_t)^{1/(2-q)} & \text{for } q \neq 2 \end{cases} \quad (11)$$

where for a jet the comoving B' value should be used.

References

- [1] Aartsen MG, et al. *Physical Review Letters* 111:021103 (2013)
- [2] IceCube Collaboration. *Science* 342 (2013)
- [3] Aartsen MG, et al. *Phys.Rev.D* 91:022001 (2015)
- [4] Gaisser T, Halzen F. *Annual Review of Nuclear and Particle Science* 64:101 (2014)
- [5] Babson J, et al. *Phys.Rev.D* 42:3613 (1990)
- [6] Avrorin AD, et al. 2016. In *European Physical Journal Web of Conferences*, vol. 116 of *European Physical Journal Web of Conferences*
- [7] Margiotta A, ANTARES Collaboration. *Journal of Physics Conference Series* 718:062041 (2016)
- [8] Aartsen MG, et al. *Astrophys.J.* 809:98 (2015)
- [9] Aartsen MG, et al. *Physical Review Letters* 114:171102 (2015)
- [10] IceCube Collaboration, et al. *ArXiv e-prints* 1609.04981 (2016)
- [11] IceCube Collaboration, Pierre Auger Collaboration, Telescope Array Collaboration. *Jour. Cosmology and Astro-Particle Phys.* 1:037 (2016)
- [12] Murase K, Waxman E. *ArXiv e-prints* 1607.01601 (2016)
- [13] Murase K, Ahlers M, Lacki BC. *Phys.Rev.D* 88:121301 (2013)
- [14] Anchordoqui LA, et al. *ArXiv e-prints* 1306.5021 (2013)
- [15] Barger V, et al. *ArXiv e-prints* 1407.3255 (2014)
- [16] Kistler MD, Laha R. *ArXiv e-prints* 1605.08781 (2016)
- [17] Sahu S, Zhang B. *ArXiv e-prints* 1612.09043 (2016)
- [18] Anchordoqui LA, et al. *ArXiv e-prints* 1611.07905 (2016)
- [19] Biehl D, et al. *ArXiv e-prints* 1611.07983 (2016)
- [20] He HN, et al. *Phys.Rev.D* 87:063011 (2013)

- [21] Liu RY, et al. *Phys.Rev.D* 89:083004 (2014)
- [22] Senno N, et al. *Astrophys.J.* 806:24 (2015)
- [23] Murase K. *AIP Conf. Proc.* 1666:040006 (2015)
- [24] Ahlers M. 2015. In *2014 Fermi Symposium proceedings - eConf C14102.1*, 8 pp.
- [25] Berezhinskii VS, Smirnov AI. *Astrophys.Space.Sci.* 32:461 (1975)
- [26] Ackermann M, et al. *Astrophys.J.* 799:86 (2015)
- [27] Liu RY, et al. *Phys.Rev.D* 89:083004 (2014)
- [28] Chang XC, Wang XY. *Astrophys.J.* 1406.1099:131 (2014)
- [29] Ando S, Tamborra I, Zandanel F. *ArXiv e-prints* (2015)
- [30] Zandanel F, Tamborra I, Gabici S, Ando S. *Astron.Astrophys.* 578:A32 (2015)
- [31] Murase K, Guetta D, Ahlers M. *Physical Review Letters* 116:071101 (2016)
- [32] Waxman E, Bahcall J. *Physical Review Letters* 78:2292 (1997)
- [33] Murase K, Ioka K. *Physical Review Letters* 111:121102 (2013)
- [34] Senno N, Murase K, Mészáros P. *Phys.Rev.D* 93:083003 (2016)
- [35] Xiao D, Mészáros P, Murase K, Dai ZG. *ArXiv e-prints* 1608.08150 (2016)
- [36] Wang XY, Liu RY. *ArXiv e-prints* 1512.08596 (2015)
- [37] Senno N, Murase K, Meszaros P. *ArXiv e-prints* 1612.00918 (2016)
- [38] Kimura SS, Murase K, Toma K. *Astrophys.J.* 806:159 (2015)
- [39] Chang XC, Liu RY, Wang XY. *ArXiv e-prints* (2016)
- [40] Xiao D, Mészáros P, Murase K, Dai ZG. *Astrophys.J.* 826:133 (2016)
- [41] Dennison Dermer C, Giebels B. *ArXiv e-prints* 1602.06592 (2016)
- [42] Protheroe RJ, Kazanas D. *Astrophys.J.* 265:620 (1983)
- [43] Biermann PL, Strittmatter PA. *Astrophys.J.* 322:643 (1987)
- [44] Stecker FW, Salamon MH. *Space Science Reviews* 75:341 (1996)
- [45] Atoyan A, Dermer CD. *Physical Review Letters* 87:221102 (2001)
- [46] Murase K, Inoue Y, Dermer CD. *Phys.Rev.D* 90:023007 (2014)
- [47] Padovani P, et al. *M.N.R.A.S.* 457:3582 (2016)
- [48] Alvarez-Muñiz J, Mészáros P. *Phys.Rev.D* 70:123001 (2004)

- [49] Pe'er A, Murase K, Mészáros P. *Phys.Rev.D* 80:123018 (2009)
- [50] Murase K. *ArXiv e-prints* 1511.01590 (2015)
- [51] Dermer CD, Murase K, Inoue Y. *Journal of High Energy Astrophysics* 3:29 (2014)
- [52] Padovani P, Petropoulou M, Giommi P, Resconi E. *M.N.R.A.S.* 452:1877 (2015)
- [53] Stecker FW. *Phys.Rev.D* 88:047301 (2013)
- [54] Becker Tjus J, et al. *Phys.Rev.D* 89:123005 (2014)
- [55] Hooper D. *ArXiv e-prints* (2016)
- [56] IceCube Collaboration, et al. *ArXiv e-prints* 1611.03874 (2016)
- [57] Neronov A, Semikoz DV, Ptitsyna K. *ArXiv e-prints* 1611.06338 (2016)
- [58] Resconi E, et al. *ArXiv e-prints* 1611.06022 (2016)
- [59] Völk HJ, Aharonian FA, Breitschwerdt D. *Space Sci. Rev.* 75:279 (1996)
- [60] Berezhinsky VS, Blasi P, Ptuskin VS. *Astrophys.J.* 487:529 (1997)
- [61] Loeb A, Waxman E. *Nature* 405:156 (2000)
- [62] Keshet U, et al. *Astrophys.J.* 585:128 (2003)
- [63] Norman CA, Melrose DB, Achterberg A. *Astrophys.J.* 454:60 (1995)
- [64] Inoue S, Aharonian FA, Sugiyama N. *Astrophys.J.Lett.* 628:L9 (2005)
- [65] Murase K, Inoue S, Nagataki S. *Astrophys.J.Lett.* 689:L105 (2008)
- [66] Zandanel F, Pfrommer C, Prada F. *M.N.R.A.S.* 438:124 (2014)
- [67] Nelson D, et al. *Astronomy and Computing* 13:12 (2015)
- [68] Kashiyama K, Mészáros P. *Astrophys.J.Lett.* 790:L14 (2014)
- [69] Murase K, Inoue S, Nagataki S. *Astrophys.J.Lett.* 689:L105 (2008)
- [70] Kotera K, et al. *Astrophys.J.* 707:370 (2009)
- [71] Ackermann M, the Fermi collab. . *Physical Review Letters* 116:151105 (2016)
- [72] Watson A. *ArXiv e-prints* (2016)
- [73] The Pierre Auger Collaboration, et al. *ArXiv e-prints* 1609.08567 (2016)
- [74] Allard D, et al. *JCAP* 0609:005 (2006)
- [75] Loeb A, Waxman E. *Jour. Cosmology and Astro-Particle Phys.* 5:3 (2006)
- [76] Waxman E, Bahcall J. *Phys.Rev.D* 59:023002 (1999)

- [77] Wang XY, Razzaque S, Meszaros P, Dai ZG. *Phys.Rev.* D76:083009 (2007)
- [78] Budnik R, Katz B, MacFadyen A, Waxman E. *Astrophys.J.* 673:928 (2008)
- [79] Tamborra I, Ando S, Murase K. *Jour. Cosmology and Astro-Particle Phys.* 9:043 (2014)
- [80] Bartos I, Marka S. *ArXiv e-prints* 1509.00983 (2015)
- [81] Hopkins AM, Beacom JF. *Astrophys.J.* 651:142 (2006)
- [82] Lacki BC, Horiuchi S, Beacom JF. *Astrophys.J.* 786:40 (2014)
- [83] Gehrels N, Ramirez-Ruiz E, Fox DB. *Annu.Rev.Astron.Astrophys.* 47:567 (2009)
- [84] Mészáros P. *Astroparticle Physics* 43:134 (2013)
- [85] Mészáros P, Rees MJ. *Astrophys.J.* 530:292 (2000)
- [86] Rees MJ, Mészáros P. *Astrophys.J.* 628:847 (2005)
- [87] Beloborodov AM. *M.N.R.A.S.* 407:1033 (2010)
- [88] Zhang B, Yan H. *Astrophys.J.* 726:90 (2011)
- [89] Murase K, Asano K, Terasawa T, Mészáros P. *Astrophys.J.* 746:164 (2012)
- [90] Waxman E, Bahcall JN. *Astrophys.J.* 541:707 (2000)
- [91] Murase K. *Phys.Rev.D* 78:101302 (2008)
- [92] Gao S, Asano K, Meszaros P. *Jour. Cosmology and Astro-Particle Phys.* 11:58 (2012)
- [93] Murase K, Kashiyama K, Mészáros P. *Physical Review Letters* 111:131102 (2013)
- [94] Bartos I, Beloborodov AM, Hurley K, Márka S. *Physical Review Letters* 110:241101 (2013)
- [95] Asano K, Meszaros P. *Astrophys.J.* 785:54 (2014)
- [96] Zhang B, Kumar P. *Physical Review Letters* 110:121101 (2013)
- [97] Aartsen MG, et al. *Astrophys.J.Lett.* 805:L5 (2015)
- [98] Ahlers M, Gonzalez-Garcia MC, Halzen F. *Astroparticle Physics* 35:87 (2011)
- [99] Abbasi R, et al. *Physical Review Letters* 106:141101 (2011)
- [100] Abbasi R, et al. *Nature* 484:351 (2012)
- [101] He HN, et al. *Astrophys.J.* 752:29 (2012)
- [102] Li Z. *Phys.Rev.D* 85:027301 (2012)
- [103] Hümmel S, Baerwald P, Winter W. *Physical Review Letters* 108:231101 (2012)
- [104] Kashiyama K, Murase K, Mészáros P. *Physical Review Letters* 111:131103 (2013)

- [105] Soderberg AM, et al. *Nature* 442:1014 (2006)
- [106] Campana S, et al. *Nature* 442:1008 (2006)
- [107] Howell EJ, Coward DM. *M.N.R.A.S.* 428:167 (2013)
- [108] Murase K, Ioka K, Nagataki S, Nakamura T. *Astrophys.J.Lett.* 651:L5 (2006)
- [109] Liu RY, Wang XY, Dai ZG. *M.N.R.A.S.* 418:1382 (2011)
- [110] Waxman E, Mészáros P, Campana S. *Astrophys.J.* 667:351 (2007)
- [111] Chevalier RA, Fransson C. *Astrophys.J.Lett.* 683:L135 (2008)
- [112] Mészáros P, Waxman E. *Physical Review Letters* 87:171102 (2001)
- [113] Aartsen MG, et al. *ArXiv e-prints* (2015)
- [114] Nakar E. *Astrophys.J.* 807:172 (2015)
- [115] Razzaque S, Mészáros P, Waxman E. *Phys. Rev.* D68:083001 (2003)
- [116] Razzaque S, Meszaros P, Waxman E. *Phys. Rev. Lett.* 93:181101 (2004)
- [117] Ando S, Beacom JF. *Physical Review Letters* 95:061103 (2005)
- [118] Horiuchi S, Ando S. *Phys.Rev.D* 77:063007 (2008)
- [119] Horiuchi S, Ando S. 2009. In *American Institute of Physics Conference Series*, ed. C. Balazs & F. Wang, vol. 1178 of *American Institute of Physics Conference Series*
- [120] Fraija N. *Journal of High Energy Astrophysics* 9:25 (2016)
- [121] Katz B, Sapir N, Waxman E. 2012. In *Death of Massive Stars: Supernovae and Gamma-Ray Bursts*, eds. P Roming, N Kawai, E Pian, vol. 279 of *IAU Symposium*
- [122] Kashiyama K, et al. *Astrophys.J.Lett.* 769:L6 (2013)
- [123] Giacinti G, Bell AR. *M.N.R.A.S.* 449:3693 (2015)
- [124] Gupta N, Zhang B. *Astroparticle Physics* 27:386 (2007)
- [125] Levinson A, Bromberg O. *Physical Review Letters* 100:131101 (2008)
- [126] Burrows DN, et al. *Nature* 476:421 (2011)
- [127] Farrar GR, Piran T. *ArXiv e-prints* 1411.0704 (2014)
- [128] Metzger BD, Stone NC. *M.N.R.A.S.* 461:948 (2016)
- [129] Dai L, Fang K. *ArXiv e-prints* 1612.00011 (2016)
- [130] Lunardini C, Winter W. *ArXiv e-prints* 1612.03160 (2016)
- [131] Beloborodov AM. *M.N.R.A.S.* 438:169 (2014)

- [132] Smith MWE, et al. *Astroparticle Physics* 45:56 (2013)
- [133] Cowen DF, Keivani A, Tešić G. 2016. In *European Physical Journal Web of Conferences*, vol. 116 of *European Physical Journal Web of Conferences*
- [134] Katz B, Waxman E, Thompson T, Loeb A. *ArXiv e-prints* 1311.0287 (2013)
- [135] Waxman E. *ArXiv e-prints* 1511.00815 (2015)
- [136] Adrián-Martínez S, et al. *Journal of Physics G Nuclear Physics* 43:084001 (2016)
- [137] The IceCube-Gen2 Collaboration, et al. *ArXiv e-prints* 1510.05228 (2015)
- [138] Shoemaker IM, Murase K. *Phys.Rev.D* 93:085004 (2016)
- [139] IceCube Collaboration, et al. *ArXiv e-prints* 1612.05949 (2016)
- [140] Aartsen MG, et al. *European Physical Journal C* 76:531 (2016)
- [141] Vieregge AG. *Nucl. Phys. Proc. Suppl.* 229-232:545 (2012)
- [142] Barwick SW, et al. *ArXiv e-prints* (2016)
- [143] Besson D, et al. *PoS ICRC2015:1105* (2016)
- [144] Ricci M. *J. Phys. Conf. Ser.* 718:052034 (2016)
- [145] Bigongiari C. *ArXiv e-prints* 1606.08190 (2016)
- [146] Giannios D. *M.N.R.A.S.* 408:L46 (2010)
- [147] Dermer CD, Miller JA, Li H. *Astrophys.J.* 456:106 (1996)
- [148] Bykov AM, Mészáros P. *Astrophys.J.Lett.* 461:L37+ (1996)
- [149] Petrosian V, Liu S. *Astrophys.J.* 610:550 (2004)
- [150] Brunetti G, Lazarian A. *M.N.R.A.S.* 378:245 (2007)